Geoscientific
Model Development
Discussions

Open Access

Tracking winter extra-tropical cyclones based on their relative vorticity evolution and sensitivity to prior data filtering (cycloTRACK v1.0)

E. Flaounas[1], V. Kotroni[2], K. Lagouvardos[2], and I. Flaounas[3]

[1]LMD/IPSL, CNRS and Ecole Polytechnique, Palaiseau, France
[2]Institute for Environmental Research and Sustainable Development, National Observatory of Athens, Athens, Greece
[3]Intelligent Systems Laboratory, University of Bristol, Bristol, UK

Correspondence to: E. Flaounas (flaounas@lmd.polytechnique.fr)

Discussion Paper | Discussion Paper | Discussion Paper | Discussion Paper

GMDD

7, 1245–1276, 2014

Tracking winter extra-tropical cyclones

E. Flaounas et al.

Title Page

Abstract	Introduction
Conclusions	References
Tables	Figures

◀◀ ▶▶

◀ ▶

Back Close

Full Screen / Esc

Printer-friendly Version

Interactive Discussion

Abstract

In this study we present a new cyclone identification and tracking algorithm. Identification is based on a recognition pattern of enclosed contours of 850 hPa filtered relative vorticity values, while tracking is based on the minimization of a cost function. In particular, for each tracked cyclone our algorithm builds all possible tracks and finally chooses the one which presents the least differences of relative vorticity between consecutive track points. In parallel, for each track point the algorithm provides a cyclone area within which different physical diagnostics are calculated (such as pressure and wind speed). The area size is a function of the cyclone relative vorticity.

To validate our approach we apply the algorithm on the Northern Hemisphere for the winters of 1989–2009. Three integrations of the algorithm were performed, each by using different filtering strengths. Using the three integrations, we assess the algorithm sensitivity to prior filtering the relative vorticity field. We show that filtering the input relative vorticity fields has an impact only on the weak cyclones, while in their majority the strong cyclones are independently detected and tracked.

1 Introduction

Identification and tracking of atmospheric features is thoroughly used for research in atmospheric sciences. Without doubt, the most investigated atmospheric features based on identification and tracking algorithms are the tropical and extra-tropical cyclones (e.g. Hodges, 1999; Blender and Schubert, 2000; Hoskins and Hodges, 2002; Ulbrich et al., 2009; Inatsu, 2009). However, several other atmospheric features are also identified and tracked in climatological datasets such as Mesoscale Convective Systems (MCS; e.g. Machado et al., 1998), conveyor belts (e.g. Eckhardt et al., 2004), cut-off lows (Wernli and Sprenger, 2007) and dry air intrusions (Roca et al., 2005; Flaounas et al., 2012).

In general, tracking diagnostic tools function in two phases. In the first phase, the algorithm has to identify the location of an atmospheric feature for a given time, while in the second, all features are tracked by connecting their identified locations in consecutive time steps. Numerous decisions have to be made during these two phases. These decisions determine the algorithm's level of flexibility. The more constraints applied in the identification phase, the narrower gets the range and number of the identified features. For instance, in some studies, the definition of the location of a cyclone applies three constraints on the fields of mean sea level pressure: (1) the representative grid point of the data field has to have the minimum value among the neighboring grid points; (2) the minimum value has to be inferior of a threshold value; and (3) the field gradient has to be superior of a threshold value (e.g. Murray and Simmonds, 1991; Blender and Schubert, 2000; Nissen et al., 2010). However, the application of "strict" constraints on pressure gradients may lead to tracking cyclones close to their mature stage, whereas weak cyclones may not be detected at all.

Once the features identification phase is completed, tracking is the most challenging task. An algorithm needs to decide on whether the identified features have been displaced in time or they have ceased to exist. That decision step becomes more complicated if a feature is split or merged, or simply, if there are more than one candidate features to consider for its next location. The latter case is found often in noisy fields, where the algorithm may identify as cyclone centers a significant number of grid points which are located close to each other. In this case, a well designed algorithm has to decide which of the candidate features in the next time steps constitute the natural evolution of the tracked feature and which should be neglected. In many methods a "nearest point" approach is applied, where feature tracks are built by connecting the identified features of a given time step with the nearest one of the following time step (Blender et al., 1997; Serreze et al., 1997; Trigo et al., 1999). In those methods, inconveniences might arise due to the wrong decisions of the algorithm between the different next time step candidate locations. Other studies use more complicated tracking algorithms based on the feature's speed (e.g. Murray and Simmonds, 1991; Wernli

et al., 2006; Davis et al., 2008; Campins et al., 2011; Hanley and Caballero, 2012). These algorithms make a "guess" of the feature's next step location and therefore they choose the nearest feature detected to this potential location. Finally, Inatsu (2009) presented an algorithm where tracking is based on neighbor enclosed area tracking. In this
5   scheme cyclones are regarded as an area of connected grids which satisfy a certain condition and they are tracked in time if the areas overlap in consecutive time-steps.

Post-treatment of the tracked features has been also proposed. In Hodges (1999), the tracking algorithm constructs all tracks using a "nearest point" method. Then, the tracks are altered by exchanging between them their track points. The algorithm contin-
10 ues to alter the tracks until a cost function is minimized. The cost function is a measure of smoothness of the total number of tracks. Hanley and Caballero (2012) apply a post treatment routine in order to identify if the cyclones which present more than one center undergo any merging or splitting process. If such processes are present during a cyclone life-time, then tracks are altered accordingly (i.e. merged or split).
15 Recently the IMILAST project presented the results from a large effort in inter-comparing the performance of 15 different tracking algorithms in tracking extra-tropical cyclones during the cold season of 21 yr over the entire planet (Neu et al., 2013). Depending on the algorithm, the tracks number, the cyclones life span or intensity might vary significantly. Indeed, there is a divergence on the algorithms results which is fun-
20 damentally based on the fact that for each algorithm the definition of a cyclone is modeled accepting different constraints and/or different fields. In this sense, one of the main results of this effort is that no algorithm is considered as "superior" or more "correct" than the others, since cyclones are not defined in the same way. It is also noticeable in Neu et al. (2013) that similar algorithms in their configuration might not present highly
25 matching results. Despite the variety of the results, Ulbrich et al. (2013) showed that the algorithms have a common behavior when considering the extra-tropical cyclones tracks evolution in the context of changing climate. This result confirms that independently of the different algorithms set-up and modeling constraints there is a common robust behavior.

In this study, our principal motivation is to design an algorithm which is able to provide qualitative characteristics of the tracked features in parallel with their tracking (splitting, merging, wind speed, associated rainfall, minimum pressure etc.). A new aspect of the proposed approach is that cyclonic features are tracked based on their physical prop-
5 erties, by assuring a gradual evolution of the cyclone relative vorticity, and not on their displacement. The use of relative vorticity presents some advantages when compared to geopotential height or mean sea level pressure since it is a high frequency variable, representative of local scales and permits the tracking of a feature presumably since its very initial perturbation, before it can be detected by closed pressure con-
10 tours (Hodges, 1999; Inatsu, 2009; Kew et al., 2010). This can be an advantage when considering for instance explosive cyclogenesis where cyclones intensity increases significantly in twenty four hours (e.g. Sanders and Gyakum, 1980; Trigo et al., 2006; Lagouvardos et al., 2007). On the other hand, relative vorticity is a wind-based field, sensitive to the dataset horizontal resolution, while local maxima might not correspond
15 to wind vortices but to other features such as an abrupt wind turning.

To deal with the spatial noise of relative vorticity, in our approach we smooth the input fields. The smoothing operation partly counteracts the advantage of relative vorticity to detect cyclones since their early stage but nevertheless we offer the algorithm a high degree of flexibility, tracking perturbations which did not evolve to strong cyclones.
20 Such a setup for capturing weak cyclonic features has been also performed by previous studies (e.g. Murray and Simmonds, 1991; Pinto et al., 2005), however in our approach this provides an added value for determining the cyclones which are not sensitive to prior filtering. The code application and assessment is done in line with the efforts of the IMILAST project, using the same time periods and input datasets, in order to make
25 the results of our algorithm comparable with those of the aforementioned project.

Section 2 describes in detail the algorithm's methodology while Sect. 3 provides the results of its application on extra-tropical cyclones over the Northern Hemisphere for the cold season (December-January-February) for the 21 yr period of 1989–2009. Finally, Sect. 4 hosts the conclusion and our prospects.

Tracking winter extra-tropical cyclones

E. Flaounas et al.

|◀ | ▶|

◀ | ▶

Back | Close

Full Screen / Esc

Printer-friendly Version

Interactive Discussion

2 Identification and tracking algorithm methodology

In this section we present the functionality of the algorithm. To better understand the different parts of the code we make a step by step application on the vorticity fields at 850 hPa level for the extra-tropical latitudes of the Northern Hemisphere during the winters of 1989–2009. Meteorological data are taken from the ERA-Interim reanalyses (ERA-I) with a horizontal resolution of 1.5° × 1.5° (ERA-I; Uppala et al., 2008). The algorithm is composed by two independent phases: in the first phase, the algorithm identifies all cyclonic features for all time steps of a dataset and in the second it builds the feature's tracks.

2.1 Phase I: identifying cyclones and quantifying their characteristics

The first phase of the algorithm is devoted to the identification of the cyclones and to the quantification of their characteristics. This is performed in three steps. First, the algorithm identifies all cyclonic features, or more precisely all cyclonic circulations. Then, for each cyclonic circulation the algorithm identifies all of its representative centers which will be treated as different cyclones. Finally, for each center, the algorithm will quantify its characteristics (e.g. maximum relative vorticity, maximum wind speed, minimum sea level pressure).

2.1.1 Identification of cyclonic circulations

In a first step, we spatially smooth the vorticity field by applying a spatial correlation filter. The application of filtering is essential first for suppressing orographic or coastal vorticity maxima and second, for providing smoother gradients of relative vorticity fields. The latter is very helpful since it helps the algorithm to reject local vorticity maxima which are nested within noisy field gradients (especially near the core center of a cyclone and when considering very high resolution datasets). The smoothing operation on the relative vorticity field is performed at each grid point separately by multiplying

the sum of all its neighboring X grid points by $1/X$. For instance at any grid point a, b the smoothed Relative Vorticity (RV) equals:

$$\frac{1}{X} \cdot \sum_{i=a-X}^{a+X} \sum_{j=b-X}^{b+X} (\text{RV}_{i,j}) \qquad (1)$$

5 As a result, the larger X is, the stronger is the smoothing operation on the relative vorticity fields. Finally, we apply a threshold value and we retain only the grid points corresponding to higher values.

Figure 1 shows the raw relative vorticity fields and the filtered ones by applying three different filters with X equal to 3, 5 and 7. The relative vorticity fields are derived from 10 ERA-I and they are centered over Europe at 00:00 UTC on the 3 December 1999, featuring the Anatol storm over Denmark as the strongest detected cyclone. In all panels of Fig. 1 the threshold is set at $3 \times 10^{-5}\,\text{s}^{-1}$. Depending on the filter strength the relative vorticity values are accordingly weakened and all small vorticity features are suppressed. Nevertheless, the structure and location of the vorticity maxima of the 15 strongest features, as the Anatol storm, are not altered among the different filter operations. In fact, filtering is used for smoothing values within a cyclonic circulation. As a result, the filtering matrix should not be much larger than the length scale of a cyclone. In that sense a 7×7 grid point filter for ERA-I means that relative vorticity is smoothed in a $10.5° \times 10.5°$ region which is certainly a large area. Hence, for the dataset used 20 in this application, 3×3 grid points (smoothing fields in a $4.5° \times 4.5°$ area) is physically more consistent with the cyclone length scales.

As shown in Fig. 1a and b, each cyclonic circulation might correspond to a unique cyclone or to a larger scale cyclonic circulation (i.e. $3 \times 10^{-5}\,\text{s}^{-1}$ enclosed contours) of more than one local maximum. The application of the $3 \times 10^{-5}\,\text{s}^{-1}$ threshold on the 25 $1.5° \times 1.5°$ dataset has been found adequate for describing cyclones even at their initial perturbation, for all filtering integrations. In this step of the algorithm, and after applying the threshold value, the algorithm identifies as a cyclonic circulation the areas composed by neighboring grid points with values above the applied threshold and labels

Full Screen / Esc

Printer-friendly Version

Interactive Discussion

them with a number (i.e. all the enclosed contours of relative vorticity above the defined threshold). Similar approaches in identifying a feature through an enclosed area have been previously used for cyclones (e.g. Hodges, 1999; Wernli et al., 2006; Inatsu, 2009; Flaounas et al., 2013) as well as for other features (e.g. for MCS in Machado et al., 1998).

2.1.2 Identification of cyclonic centers

It is evident in Fig. 1b–d that not all cyclonic circulations correspond to a unique cyclone. For this reason each labeled cyclonic circulation is further treated by locating all local vorticity maxima within the cyclonic circulation. These local maxima will be also labeled and eventually will be treated as the centers of unique cyclones. The term "centers of unique cyclones" has no physical basis but is conveniently used here in order to describe the grid points which present local maxima of relative vorticity and are followed in time in order to construct the cyclones tracks. In this sense we need to provide the algorithm with a representative cyclone center even though the cyclone structure might be very complex with more than one vorticity maximum, especially in very high resolution datasets. To deal with this issue, (1) we filter the data, smoothing the noisy gradients (already performed in the previous step), (2) we define the local maxima as the maximum value of the central grid point among its eight surrounding grid points and (3) we consider that between two centers there is a relative vorticity difference greater than the threshold value which is applied to define the cyclonic circulations (in this case the difference is of at least $3 \times 10^{-5}\,\mathrm{s}^{-1}$). The last criterion prohibits the weaker cyclonic circulations (i.e. identified cyclones of relative vorticity close to the threshold value) to present multiple centers. Indeed, accepting the threshold value as our fundamental criterion for separating cyclones from the rest of the atmospheric circulation, two cyclones within a larger cyclonic circulation must differ by embedded enclosed contours where their maxima and lateral contours have a difference of at least the threshold value. Figure 1 shows the different maxima identified in the raw and filtered relative vorticity fields. It is evident that the number of the cyclone centers diminishes proportionally

to the filter strength. Indeed, smoothing the relative vorticity fields has the effect of reducing the vorticity values and thus the gradients strength within the identified cyclonic circulations. As a result, the number of embedded cyclonic centers is reduced especially due to our third criterion.

2.1.3 Quantifying cyclone characteristics

Once all cyclones have been identified, we determine an "effective area" for each cyclone. This area is a circular disk centered on the cyclone vorticity maximum as identified in the previous step. The disk radius grows gradually until: (1) all grid points included in the disk have a vorticity average inferior to a threshold value or (2) until the radius reaches a pre defined maximum length or (3) until a higher than that of the cyclonic center relative vorticity value is found within the area. According to this empirical methodology, strong or large (but weak) cyclones tend to produce large effective areas. The third criterion favors the stronger cyclones to spread their area independently of the presence of other weaker ones in their region, while it restrains the weaker cyclones not to share atmospheric fields with the strong cyclones. In Flaounas et al. (2013) the cyclone area was defined by the cyclone enclosed contour as defined by the applied threshold value (see their appendix figure). However, such an enclosed area might not capture grid points which present lower than the applied threshold relative vorticity values. In Lim and Simmonds (2007) the cyclone area was also defined by a representative circular disk of a radius which derived by the average distance between the cyclone center and the enclosing zero contour of the mean sea level pressure laplacian. In our algorithm the circular disk seemed the best choice of capturing the affected areas by a cyclonic vortex, although more "irregular shapes" might be considered as for instance enclosed contours of pressure (Wernli et al., 2006; Hanley and Caballero, 2012) or of relative vorticity (Flaounas et al., 2013).

Once the effective area is defined, our algorithm computes the physical properties of the cyclone within the area's grid points. Among the physical properties, the maximum wind speed and pressure gradient, and total precipitation, are included. As an example,

Fig. 2 shows the effective area and the detection of the minimum sea level pressure and the maximum 10 m wind of the storm Anatol at the same time as in Fig. 1b.

2.2   Phase II: tracking cyclones

Before the start of the tracking phase, our algorithm sorts the identified cyclones based on their relative vorticity value, from the strongest (i.e. the one with the highest relative vorticity value) to the weakest. Then, it starts from the first cyclone and searches forward and backward in time for all its undergoing possible tracks. More precisely, the algorithm constructs all possible cyclone tracks which present the same highest vorticity state. Once all possible tracks are constructed, the algorithm chooses the track for which the feature presents the most "natural evolution" of relative vorticity, i.e. the track which presents the smallest differences of relative vorticity in consecutive points, weighted by the distance between the track point locations.

Figure 3a illustrates an idealized experiment, presenting the locations of all identified cyclones in a four time step dataset. Six cyclones are identified: one cyclone in the first time step, one cyclone in the second time step and two cyclones for each of the time steps three and four. The tracking process begins from the strongest cyclone (i.e., the cyclone 2(12)) and constructs all possible tracks by iterating forward and backward in time with all other features. Figure 3b shows that the first cyclone may undertake four possible tracks, however it is obvious that the track 1(9), 2(12), 3(10), 4(8) presents the most "natural evolution", since maximum relative vorticity differs the least from one time step to the next. The algorithm saves this track and deletes the used cyclones' locations from the dataset. Then, a new iteration begins where the algorithm will start from the cyclone with highest vorticity and eventually a new track will be constructed (Fig. 3c). Starting the tracks from the cyclone's highest vorticity state was found very convenient for reducing the mistakes in the beginning of the trajectories construction step. Indeed, in the previous and next time step of the cyclone with the highest vorticity state, for most cases, there is only one strong cyclone to act as a candidate for continuing the tracks.

Tracking winter extra-tropical cyclones

E. Flaounas et al.

The practice of minimizing cost functions, has been used before by Hodges (1995, 1999), who builds the feature tracks by minimizing the cost function of the feature's trajectory smoothness. Here, the feature's evolution in each track is determined by a cost function (C), represented by the absolute average difference of relative vorticity weighted by the distance between two consecutive time steps:

$$C = \sum_{n=1}^{n=N-1} d_{n \to n+1}(|V_{n+1} - V_n|) \qquad (2)$$

where C is the cost function of a candidate track, N is the total number of the track's time steps, d is the distance between two consecutive track points and V is the relative vorticity at each time step. Performing sensitivity tests by altering Eq. (2), we found that the term d did not add significantly to the performance of the algorithm. However, for certain cases it seemed useful to weight the vorticity differences by the distance, especially when the candidate cyclones presented similar vorticity with the tracked cyclone, but were located unrealistically far from the tracked cyclone.

The number of possible tracks is quite large. However, their number can be significantly reduced by the application of a series of legitimate heuristics, that remove those tracks that present a non-natural behavior: (1) from each time step to the next, the location of the next candidate cyclone must be within a threshold range, (2) the maximum vorticity between the tracked cyclone and a candidate cyclone must not differ more than 50 % and (3) if the displacement is more than 3° for two successive displacements, then the angle between these displacements must be greater than 90°. The first constraint prohibits the algorithm from searching for next step candidate features in locations where the tracked cyclone could by no means be displaced. In our algorithm the cyclones are searched within a 5° × 10° latitude-longitude range which is the largest possible for extratropical cyclones displacement as proposed by Hodges (1999). The second constraint prohibits the algorithm from choosing candidates which consist by no means a possible evolution of the tracked feature. The use of a percentage is highly convenient since large vorticity values are subject to higher changes

Full Screen / Esc

Printer-friendly Version

Interactive Discussion

between consecutive time steps compared to small vorticity values. Finally, the third constraint prohibits the algorithm to take into account abrupt backs-and-forths of the cyclone's movement. Such displacements are more likely to take place in raw vorticity fields, where local maxima might change abruptly. For instance the algorithm would not choose the track 2(12), 3(4) and 4(8) in Fig. 3 since the consecutive displacements present an angle of 74° (marked in red in Fig. 3) which is smaller than 90°.

Finally, our algorithm returns as output a matrix for each track, containing information on the cyclone's track and physical characteristics. The matrix has a number of rows which is equal to the track points and a number of columns equal to the algorithm standard outputs plus the number of physical diagnostics. The optional output diagnostics might vary depending on the study needs and the data inputs. Labeling the cyclonic circulations (Sect. 2.1.1) and the cyclonic centers (Sect. 2.1.2) within the tracks permits a post-treatment analysis for determining merging and splitting of cyclones. For our application on the extra-tropical cyclones only maximum 10 m wind speed and sea level pressure minima are considered. As an example of the algorithm performance, Fig. 4 presents two cyclone tracks which evolve by sharing the same cyclonic circulation. The tracks are supported by the physical characteristics of the cyclones (evolution of relative vorticity, maximum 10 m wind speed and minima of sea level pressure), demonstrated in Fig. 5.

3 Applying and calibrating the tracking algorithm in a climatological context

In this section we present the results from three algorithm integrations for all winters (December, January and February) of the period 1989–2009. The three integrations differ on the use of the initial filtering of the relative vorticity field. The applied spatial filters (described in Sect. 2.1.1) correspond to a 3×3, a 5×5 and a 7×7 grid points filtering, forming three integrations named *filter3*, *filter5* and *filter7*, respectively. For all integrations the threshold used to define cyclones is $3 \times 10^{-5}\,\mathrm{s}^{-1}$. For this analysis only

tracks of at least one day life time are considered (i.e. tracks with at least four time steps).

3.1 Algorithm sensitivity on filtering

Figure 6 presents the number of cyclonic centers in function of their relative vorticity value for all three algorithm integrations. Since all integrations are bounded to identify cyclones from a common threshold of $3 \times 10^{-5} \, s^{-1}$ and since filtering decreases the relative vorticity values, due to its smoothing operation, it is of no surprise that the total number of cyclone centers is reduced with increasing filtering intensity. Regardless the integration, the forms of the three histograms in Fig. 6 seem to be similar. Indeed, calculating the average relative vorticity distance between the histogram of *filter7* and the histogram *filter3* we found $7.7 \times 10^{-5} \, s^{-1}$ and between *filter5* and *filter7* we found $2.8 \times 10^{-5} \, s^{-1}$. For both average differences the standard deviation is less than $10^{-5} \, s^{-1}$.

Strong filtering vs. weak filtering should have two effects: first it tends to detect fewer tracks, which also correspond to the stronger cyclones, and second it tends to reduce the cyclone track lengths (by not taking into account the weakest vorticity perturbations in the early and late stages of a cyclone track). The validity of the first hypothesis is evident from Fig. 1 where smoothing suppresses many weak cyclonic centers but stronger cyclones (such as the Anatol storm) are equally detected by all three integrations. To verify the second hypothesis we investigate the characteristics of the tracks as detected by *filter3*, *filter5* and *filter7*. Figure 7a–c show the Probability Distribution Function (PDF) for the life-time of tracks, the average speed of cyclones and their maximum relative vorticity. According to the results, no significant changes between the different algorithm integrations are observed when considering the cyclone life-time. Consequently the second hypothesis that average track characteristics are sensitive to the filtering can be rejected. It is interesting though that algorithm integration with weak filtering detects weak cyclones which have similar life scales. The fact that the PDF of the average speed of cyclones in Fig. 7b is also similar for all integrations means that the weaker cyclones in *filter3* and *filter5* do not correspond to weak stationary vorticity

perturbations, but nevertheless do not evolve to strong extra-tropical cyclones. An interesting question which might arise is why the weaker cyclones which are detected in *filter3* and *filter5* integrations do not evolve into strong cyclones, however, this issue is out of the scope of this paper.

In order to verify the cyclone tracks location, Fig. 8 shows the Cyclones Center Density (CCD) for all three integrations. In agreement with Fig. 6, different magnitudes of CCD are observed, depending on the filtering strength. However, the spatial pattern remains coherent for all three cases, meaning that the weakest cyclones detected in *filter3* and *filter5* (compared to *filter7*) are not orographic or coastal stationary relative vorticity perturbations. The effect of filtering (for instance *filter7* respect to *filter3*) is characteristic to the CCD within the Mediterranean region, where the cyclones are known to be weaker (Campa and Wernli, 2012) than the other extratropical cyclones forming over the oceans. Indeed, applying a strong threshold there is a dramatic decrease of detected cyclones over the Mediterranean Sea. Figure 8 presents a high similarity with the results from other algorithms (Neu et al., 2013) independently if initial filtering is performed or if sea level pressure or relative vorticity is used as input for the detection of cyclones. Indeed CCD maxima are distinctly located over the Pacific Ocean, the Northern Atlantic Ocean, and the Mediterranean. Furthermore, regardless of the integration both speed and life time PDFs (Fig. 7a and b) seem to be in good agreement with the other algorithms (Neu et al., 2013) presenting most probable cyclone speeds between 30 to $40\,\mathrm{km\,h^{-1}}$ and cyclone life time PDF decreasing exponentially from < 2 days up to a total of approximately 8 days.

3.2 Calibrating the algorithm

Figure 9 presents the interannual distribution of the number of cyclone centers which resulted from the three integrations. For all three filters, our results are in agreement with those of Neu et al. (2013) showing no specific inter-annual trend. As expected, the cyclone center number per year depends on the filtering strength. The cyclone center numbers decrease from approximately $9000\,\mathrm{yr^{-1}}$ for *filter3* to approximately $3000\,\mathrm{yr^{-1}}$

Full Screen / Esc

Printer-friendly Version

Interactive Discussion

for *filter7*. All three integrations are within the ranges of other algorithms which range from $2000\,\text{yr}^{-1}$ to $12\,000\,\text{yr}^{-1}$ but it is only *filter5* which is consistent with the majority of other algorithm results which calculated 4000 to 7000 cyclonic centers per year.

One question, which points directly at the robustness of the algorithm results and its sensitivity to initial filtering, is if the results of filter3 and filter5 would converge with those of filter7 if weak cyclones are omitted. We use *filter7* as a reference for our analysis since it presents the strongest filtering and thus the smallest number of cyclones. Then, taking into account the fact that Fig. 6 shows a constant cyclone center intensity difference between the distributions of different algorithm integrations ($7.7 \times 10^{-5}\,\text{s}^{-1}$ between *filter3* and *filter7* and $2.8 \times 10^{-5}\,\text{s}^{-1}$ between *filter5* and *filter7*) we apply these differences as thresholds in order to exclude from *filter3* and *filter5* the tracks that did not reach such high intensities. In other words, we exclude in *filter3* and *filter5* all tracks which did not reach relative vorticity values of at least $3 + 7.7 \times 10^{-5}\,\text{s}^{-1}$ and $3 + 2.8 \times 10^{-5}\,\text{s}^{-1}$, respectively. Adding $3 \times 10^{-5}\,\text{s}^{-1}$ is essential since this is the basis threshold value to identify a cyclone and since this threshold is applied after filtering the raw relative vorticity fields. The results from excluding cyclone tracks from the *filter3* and *filter5* total cyclone center number are shown in Fig. 9 (in dashed lines). After excluding weak cyclone tracks, both new cyclone center counts for *filter3* and *filter5* converge approximately on the exact same value, which is also consistent with the majority of the other algorithms presented in Neu et al. (2013). However, both new cyclone center counts do not converge with *filter7*. This is due to the fact that we only exclude from the counting all the cyclonic centers of the tracks with maximum relative vorticity smaller than the cut-off value and not all cyclonic centers with vorticity below the cut-off value. This is a logical operation that we apply since we are not interested in getting the exact same distribution of cyclonic centers but we seek in getting cyclone tracks which present similar characteristics in intensity for all three integrations. Indeed, Fig. 7d shows that the PDF of the tracks maximum relative vorticity for *filter3* and *filter5* present now a similar structure after excluding the weaker tracks (displaced in stronger relative vorticity for *filter3*) (Fig. 7d respect to Fig. 7c). Indeed, cyclone tracks

are constructed around the track point of highest relative vorticity, while other track points present a smoothed evolution of decreasing relative vorticity. As a result, one of the advantages of the algorithm is that cyclone tracks distribution can be calibrated by taking into account only their maximum relative vorticity.

5   The initial filtering in our approach functions as a spatial smoothing operator, based on the number of grid points within a square area. As a result, if the grid of our input dataset was of sufficiently fine horizontal resolution in order to permit many filtering matrix sizes, there would be an "optimal" filtering. This optimal filtering would be such that after applying the above methodology, then all cyclone center number distributions

10   from weaker filtering would be reduced to the distribution of the optimal filtering. In any case, however, the track results given by weaker filtering should not be interpreted as "wrong". In fact, they should be treated as weak cyclones which are sensitive to the strength of the filtering. In contrast, the cyclone tracks remaining after rejecting the weaker ones can be considered as independent of the filtering. What should be

15   considered as a strong or weak filtering is certainly dependent on the spatial resolution of the input dataset.

3.3 Physical coherence of the tracked cyclones

In this section we perform an analysis of the effective area diagnostic tool (described in Sect. 2.1.3) by retaining only the cyclone tracks of the *filter3* integration after calibrat-

20   ing its results (i.e. taking into account the dashed lines of *filter3* in Fig. 9). Figure 10 presents the composite evolution of the cyclones physical characteristics, centered on the time of maximum vorticity of the tracks (mature state) and averaged for all tracks detected in the Pacific Ocean (from 130° to 240° of longitude and from 30° to 90° of latitude), North Atlantic Ocean (from 300° to 360° of longitude and from 30° to 90° of

25   latitude) and within the Mediterranean region (from 345° to 45° of longitude and from 25° to 50° of latitude). The results show that regardless of the region there is a strong coherence between the evolution of sea level pressure minima, relative vorticity and maximum 10 m wind speed. The strength of the cyclones tends to increase rapidly but

decays in a slower rate. This slow weakening of the cyclones' intensity in the composite time series of Fig. 10 is due to the fact that the duration of the cyclones mature state is highly variable (as shown in Fig. 7). Here, for the construction of the composites there is no distinction depending on the cyclones life time, while one should note that the fur-
5   ther we get from the time of the cyclone maximum vorticity (i.e. the composite centers) the fewer cyclones last long enough in order to provide diagnostics for the composites. For instance, the Mediterranean cyclones life-time scale is inferior from the other extra-tropical cyclones and rarely exceeds 2–3 days. Nevertheless, our purpose here is to assess the validity of the effective area diagnostic which seems to capture cor-
10 rectly the evolution of cyclones physical characteristics regardless the region. Indeed, in agreement with Campa and Wernli (2012), Mediterranean cyclones are less deep, in terms of sea level pressure, while Atlantic cyclones are slightly deeper than the ones occurring over the Pacific Ocean.

4   Discussion and prospects

15 In this article we presented a new algorithm for identifying and tracking cyclones. The developed algorithm has been applied for the identification of winter extra-tropical cy-clonic systems over the Northern Hemisphere. The algorithm was integrated with three different initial filtering of the high frequency relative vorticity fields. The results showed that the number of tracks were inversely proportional to the filter strength. However, for
20 all three algorithm integrations the results showed coherent cyclone spatial and tempo-ral variability when compared with the results of other tracking algorithms presented in the literature. Furthermore, we showed that weak filtering makes the algorithm able to detect more cyclones but post-treatment of the tracking results provides robust results on the tracks independently of the initial filtering of the input fields. Finally, the algorithm
25 was shown to successfully capture the physical characteristics of cyclones.

Our motivation while developing the identification and tracking algorithm for cy-clones was to apply the fewer constraints possible, not only for tracking weak vorticity

perturbations which evolved in strong cyclones, but also for tracking weak perturbations that did not evolve into strong cyclones. This permits the better calibration of the algorithm, but also – in a future work – the more precise description of the environmental conditions which favor cyclogenesis and cyclone evolution. Furthermore, we chose the vorticity criteria to vary dynamically (vorticity must not vary more than 50 % in consecutive time steps) and we avoided any threshold or cut-off values which would prohibit tracking cyclones of "anomalous behavior". It should be noted that although in this study we applied the algorithm based on relative vorticity to identify and track cyclones, the same algorithm might be applied on any dataset which presents enclosed areas after applying a threshold value. For instance the algorithm could be applied on datasets of brightness temperature or cloud cover for tracking supercells or mesoscale convective systems.

Tracking uses a cost minimization approach, solely based on the cyclone relative vorticity maxima. In our experiments, rarely did the code presented more than 10–20 alternative tracks for a single cyclone, and in the majority of cases, the algorithm has chosen the correct track. Mistakes were observed especially when cyclonic circulations were found to be very noisy with multiple local maxima. As an alternative to the vorticity-based cost function used here, it would be interesting to use the weighted mean differences of additional cyclone physical characteristics (pressure, wind speed etc.) between consecutive time steps. This has been previously applied by Machado et al. (1998) for tracking MCS using brightness temperature satellite observations. However, this method would suppose an a-priori choice of the weighting value, risking restraining the code adaptability to track cyclones of different origin (e.g. extra-tropical and tropical cyclones).

The proposed algorithm links representative centers in consecutive time steps in contrast with the alternative configuration proposed by Machado et al. (1998) and Inatsu (2009) to link enclosed areas. This decision was made because if enclosed areas were linked, then large cyclonic circulations would not correspond to a single cyclone and additional criteria – and/or filtering – would be needed, while weak cyclones

would be neglected. At this point it should be noted that the extension of our algorithm to the vertical direction has been also explored. The preliminary results of the application of the tracking algorithms in three dimensions presented good skill only for the tropics. The presence of planetary waves in the mid latitudes imposed large structures of high relative vorticity values in the mid-to-high atmospheric levels which were not easily separated from the cyclones vertical structure.

Further development of the algorithm includes (1) extension of the identification part in three dimensions by searching geopotential height minima over and within the effective area and (2) extension of the code adaptability for different atmospheric features such as MCS. The code will be applied in priority for the analysis of weather extremes with special focus on the Mediterranean. More specifically merging and splitting diagnostics and the determination of more complex cyclone physical characteristics, such as temperature gradients in order to define frontal regions within the cyclones area, are the subject of the authors future work. Finally, the algorithm source is freely available in MatLab code upon request to the corresponding author.

References

Allen, J. T., Pezza, A. B., and Black, M. T.: Explosive cyclogenesis: a global climatology comparing multiple reanalyses, J. Climate, 23, 6468–6484, doi:10.1175/2010JCLI3437.1, 2010.

Blender, R. and Schubert, M.: Cyclone tracking in different spatial and temporal resolutions, Mon. Weather Rev., 128, 377–384, 2000.

Blender, R., Fraedrich, K., and Lunkeit, F.: Identification of cyclone-track regimes in the north atlantic., Q. J. R. Meteor. Soc., 123, 727–741, doi:10.1002/qj.49712353910, 1997.

Èampa, J. and Wernli, H.: A PV perspective on the vertical structure of mature midlatitude cyclones in the Northern Hemisphere, J. Atmos. Sci., 69, 725–740, doi:10.1175/JAS-D-11-050.1, 2012.

Campins, J., Genoves, A., Picornell, M. A., and Jansa, A.: Climatology of Mediterranean cyclones using the ERA-40 dataset, Int. J. Climatol., 31, 1596–1614, doi:10.1002/joc.2183, 2011.

Davis, C. A., Snyder, C., and Didlake, A.: A vortex-based perspective of eastern Pacific tropical cyclone formation, Mon. Weather Rev., 136, 2461–2477, doi:10.1175/2007MWR2317.1, 2008.

Eckhardt, S., Stohl, A., Wernli, H., James, P., Forster, C., and Spichtinger, N.: A 15-year climatology of warm conveyor belts, J. Climate, 17, 218–237, 2004.

Flaounas, E., Janicot, S., Bastin, S., Roca, R., and Mohino, E.: The role of the Indian monsoon onset in the West African monsoon onset: observations and AGCM nudged simulations, Clim. Dynam., 38, 965–983, doi:10.1007/s00382-011-1045-x, 2012.

Flaounas, E., Drobinski, P., and Bastin, S.: Dynamical dowscaling of IPSL-CM5 CMIP5 historical simulations over the Mediterranean: benefits on the representation of regional surface winds and cyclogenesis, Clim. Dynam., 40, 2497–2513, doi:10.1007/s00382-012-1606-7, 2013.

Hanley, J. and Caballero, R.: Objective identification and tracking of multicentre cyclones in the ERA-Interim reanalysis dataset, Q. J. R. Meteor. Soc., 138, 612–625, doi:10.1002/qj.948, 2012.

Hodges, K. I.: A general method for tracking analysis and its application to meteorological data, Mon. Weather Rev., 122, 2573–2586, 1994.

Hodges, K. I.: Feature tracking on the unit sphere, Mon. Weather Rev., 123, 3458–3465, 1995.

Hodges, K. I.: Adaptive constraints for feature tracking, Mon. Weather Rev., 127, 1362–1373, 1999.

Hoskins, B. J. and Hodges, K. I.: New perspectives on the Northern Hemisphere winter storm tracks, J. Atmos. Sci., 59, 1041–1061, 2002.

Inatsu, M.: The neighbor enclosed area tracking algorithm for extratropical wintertime cyclones, Atmos. Sci. Lett., 10, 267–272, doi:10.1002/asl.238, 2009.

Kew, S. F., Sprenger, M., and Davies, H.C.: Potential vorticity anomalies of the lowermost stratosphere: a 10-yr winter climatology, Mon. Weather Rev., 138, 1234–1249, 2010.

Tracking winter extra-tropical cyclones

E. Flaounas et al.

Title Page

Abstract | Introduction

Conclusions | References

Tables | Figures

◀ | ▶

◀ | ▶

Back | Close

Full Screen / Esc

Printer-friendly Version

Interactive Discussion

Lagouvardos, K., Kotroni, V., and Defer, E.: The 21–22 January 2004 explosive cyclogenesis over the Aegean Sea: observations and model analysis, Q. J. R. Meteor. Soc., 133, 1519–1531, doi:10.1002/qj.121, 2007.

Lim, E. P. and Simmonds, I.: Southern Hemisphere winter extratropical cyclone characteristics and vertical organization observed with the ERA-40 Data in 1979–2001, J. Climate, 20, 2675–2690, 2007.

Machado, L. A. T., Rossow, W. B., Guedes, R. L., and Walker, A. W.: Life cycle variations of mesoscale convective systems over the Americas, Mon. Weather Rev., 126, 1630–1654, 1998.

Murray, R. J. and Simmonds, I.: A numerical scheme for tracking cyclone centres from digital data, Part I: Development and operation of the scheme, Aust. Meteorol. Mag., 39, 155–166, 1991.

Neu, U., Akperov, M. G., Bellenbaum, N., Benestad, R., Blender, R., Caballero, R., Cocozza, A., Dacre, H. F., Feng, Y., Fraedrich, K., Grieger, J., Gulev, S., Hanley, J., Hewson, T., Inatsu, M., Keay, K., Kew, S. F., Kindem, I., Leckebusch, G. C., Liberato, M. L. R., Lionello, P., Mokhov, I. I., Pinto, J. G., Raible, C. C., Reale, M., Rudeva, I., Schuster, M., Simmonds, I., Sinclair, M., Sprenger, M., Tilinina, N. D., Trigo, I. F., Ulbrich, S., Ulbrich, U., Wang, X. L., and Wernli, H.: IMILAST: a community effort to intercompare extratropical cyclone detection and tracking algorithms, B. Am. Meteorol. Soc., 94, 529–547, 2013.

Nissen, K. M., Leckebusch, G. C., Pinto, J. G., Renggli, D., Ulbrich, S., and Ulbrich, U.: Cyclones causing wind storms in the Mediterranean: characteristics, trends and links to large-scale patterns, Nat. Hazards Earth Syst. Sci., 10, 1379–1391, doi:10.5194/nhess-10-1379-2010, 2010.

Pinto, J. G., Spangehl, T., Ulbrich, U., and Speth, P.: Sensitivities of a cyclone detection and tracking algorithm: individual tracks and climatology, Meteorol. Z., 14, 823–838, 2005.

Roca, R., Lafore, J. P., Piriou, C., and Redelsperger, J. L.: Extratropical dry-air intrusions into the West African Monsoon Midtroposphere: an important factor for the convective activity over the Sahel, J. Atmos. Sci., 62, 390–407, 2005.

Sanders, F. and Gyakum, J. R.: Synoptic-dynamic climatology of the "bomb", Mon. Weather Rev., 108, 1589–1606, 1980.

Serreze, M., Carse, F., Barry, R., and Rogers, J.: Icelandic low cyclone activity: climatological features, linkages with the NAO, and relationships with recent changes in the Northern Hemisphere circulation, J. Climate, 10, 453–464, 1997.

Tracking winter extra-tropical cyclones

E. Flaounas et al.

Title Page

Abstract | Introduction

Conclusions | References

Tables | Figures

◀◀ | ▶▶

◀ | ▶

Back | Close

Full Screen / Esc

Printer-friendly Version

Interactive Discussion

Trigo, I. F.: Climatology and interannual variability of stormtracks in the Euro-Atlantic sector: a comparison between ERA-40 and NCEP/NCAR reanalyses, Clim. Dynam., 26, 127–143, 2006.

Trigo, I., Davies, T., and Bigg, G.: Objective climatology of cyclones in the Mediterranean region, J. Climate, 12, 1685–1696, 1999.

Ulbrich, U., Leckebusch, G. C., and Pinto, J. G.: Extra-tropical cyclones in the present and future climate: a review, Theor. Appl. Climatol., 96, 117–131, doi:10.1007/s00704-008-0083-8, 2009.

Ulbrich, U., Leckebusch, G. C., Grieger, J., Schuster, M., Akperov, M., Bardin, M. Y., Feng, Y., Gulev, S., Inatsu, M., Keay, K., Kew, S. F., Liberato, M. L. R., Lionello, P., Mokhov, I. I., Neu, U., Pinto, J. G., Raible, C. C., Reale, M., Rudeva, I., Simmonds, I., Tilinina, N. D., Trigo, I. F., Ulbrich, S., Wang, X. L., and Wernli, H.: Are greenhouse gas signals of Northern Hemisphere winter extra-tropical cyclone activity dependent on the identification and tracking methodology?, Meteorol. Z., 22, 61–68, doi:10.1127/0941-2948/2013/0420, 2013.

Uppala, S., Dee, D., Kobayashi, S., Berrisford, P., and Simmons, A.: Towards a climate data assimilation system: status update of ERA-interim, ECMWF Newsletter, 115, 12–18, 2008.

Wernli, H. and Schwierz, C.: Surface cyclones in the ERA-40 dataset, part I, novel identification method and flobal climatology, J. Atmos. Sci., 63, 2486–2507, 2006.

Wernli, H. and Sprenger, M.: Identification and ERA-15 climatology of potential vorticity streamers and cutoffs near the extratropical tropopause, J. Atmos. Sci., 64, 1569–1586, 2007.

Title Page

Abstract | Introduction

Conclusions | References

Tables | Figures

|◄ | ►|

◄ | ►

Back | Close

Full Screen / Esc

Printer-friendly Version

Interactive Discussion
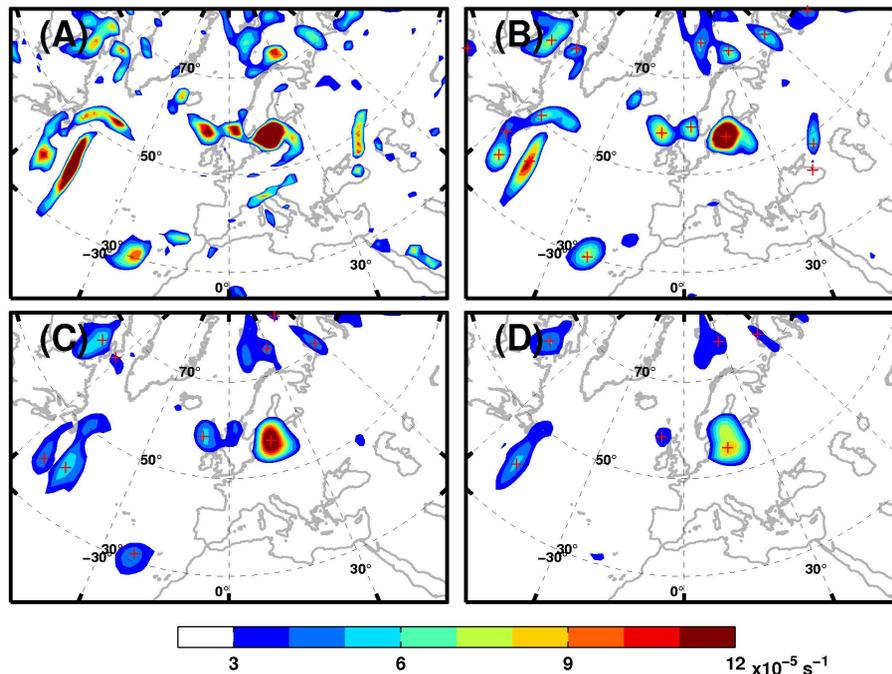
Fig. 1. (A) Relative vorticity raw fields at 00:00 UTC, 3 December 1999. The threshold applied is $3 \times 10^{-5} \, \text{s}^{-1}$. Crosses represent the central maxima located in the center of a 3×3 grid point area. **(B)** as in **(A)** but relative vorticity field is filtered using a 3×3 correlation spatial filter. **(C)** as in **(A)** but relative vorticity field is filtered using a 5×5 correlation spatial filter. **(D)** as in **(A)** but relative vorticity field is filtered using a 7×7 correlation spatial filter.

Title Page

Abstract · Introduction

Conclusions · References

Tables · Figures

|◄ · ►|

◄ · ►

Back · Close

Full Screen / Esc

Printer-friendly Version

Interactive Discussion
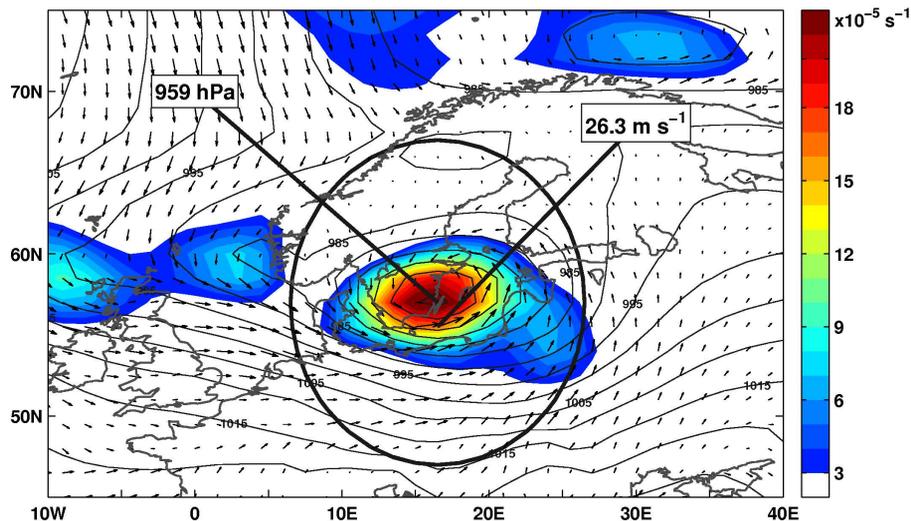
Fig. 2. The Anatol storm at 00:00 UTC, 3 December 1999. Relative vorticity smoothed by a 3×3 spatial filtering (*color*), mean sea level pressure (*in contour*) and 10 m wind field (*in arrows*). Thick black contour represents the cyclone effective area. Locations and values of maximum wind speed and lower pressure is depicted by the thick lines.
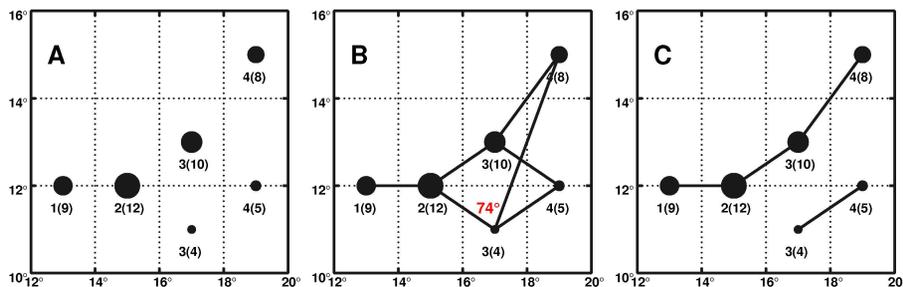
Fig. 3. (A) An idealized case of cyclone locations in four time steps. Locations are depicted by *circles*. Numbers above the locations are in the form X(Y), where *X* denotes the time step and *Y* the maximum relative vorticity. Circles size is proportional to the cyclones maximum relative vorticity value. **(B)** all possible trajectories of cyclone 2(12) searching backwards and forward in time. **(C)** Tracks results after retaining in *B* the track which presents the minimum average change of relative vorticity in successive time steps.

Full Screen / Esc

Printer-friendly Version

Interactive Discussion
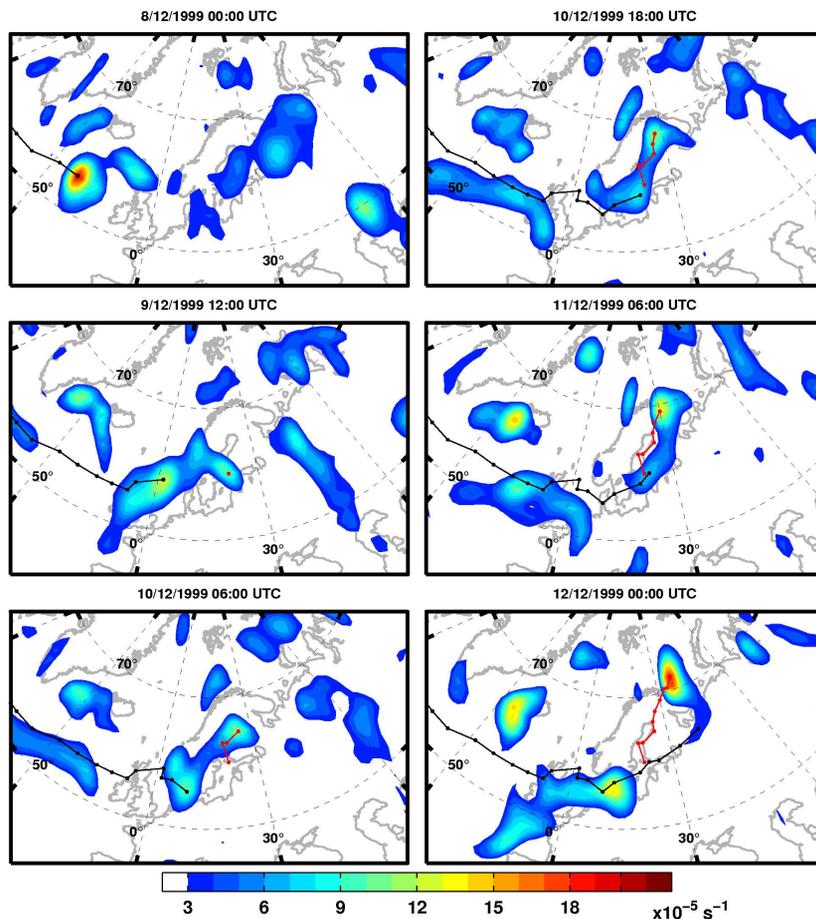
Fig. 4. Relative vorticity smoothed by a 3 × 3 spatial filter (*color*), and tracks (thin lines) of two splitting cyclones for different time frames in December 1999.

Tracking winter extra-tropical cyclones

E. Flaounas et al.

Title Page

Abstract | Introduction

Conclusions | References

Tables | Figures

|◄ | ►|

◄ | ►

Back | Close

Full Screen / Esc

Printer-friendly Version

Interactive Discussion
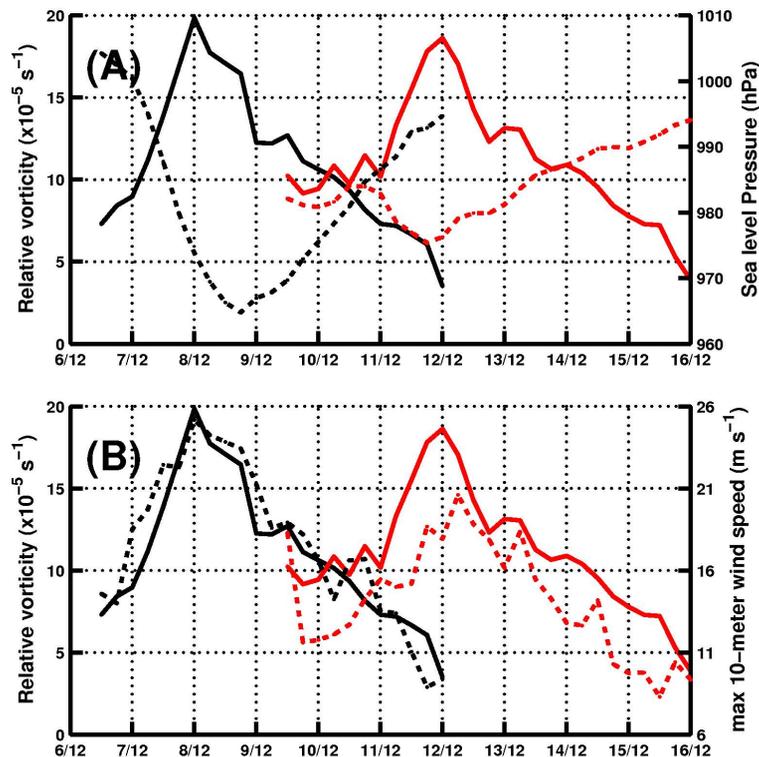
Fig. 5. (A) Maximum relative vorticity (solid line) at the tracks centers and minimum sea level pressure (dashed line) as detected within the cyclones effective area for the two splitting cyclones shown in Fig. 4b as in **(A)** but dashed line corresponds to maximum 10 m wind speed. Color lines are the same as in the tracks in Fig. 4. The horizontal axes represent the period 6–16 December 1999.

Title Page

Abstract | Introduction

Conclusions | References

Tables | Figures

|◄ | ►|

◄ | ►

Back | Close

Full Screen / Esc

Printer-friendly Version

Interactive Discussion
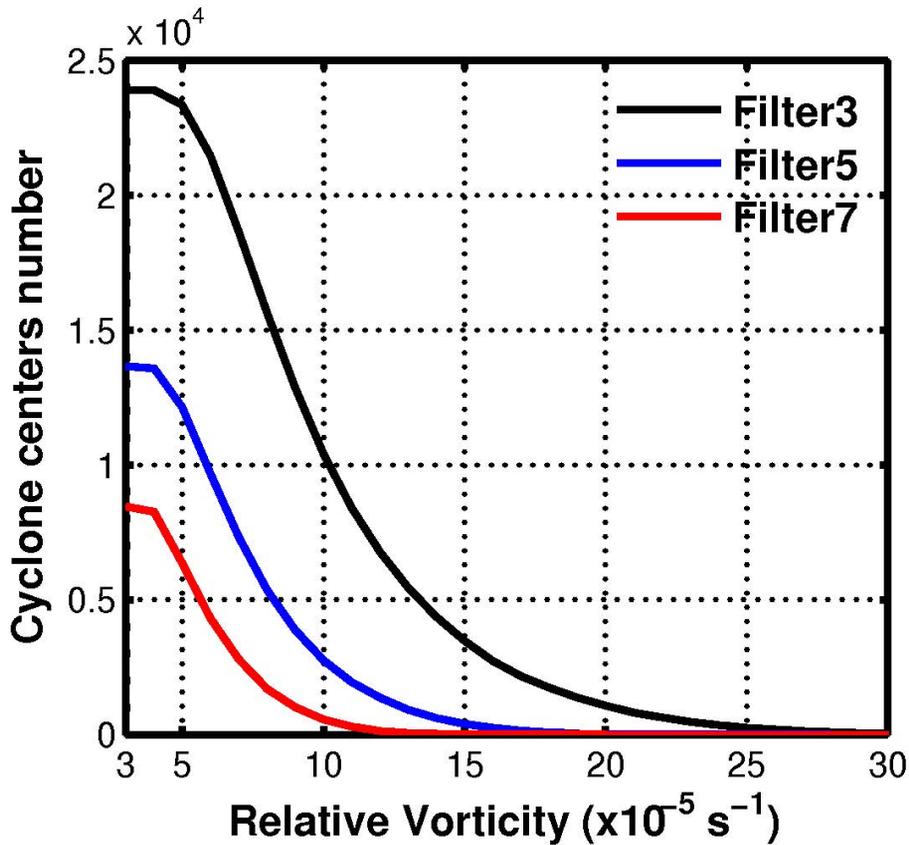
Fig. 6. Number of cyclonic centers in function of their relative vorticity value as detected by applying the three algorithm integrations.
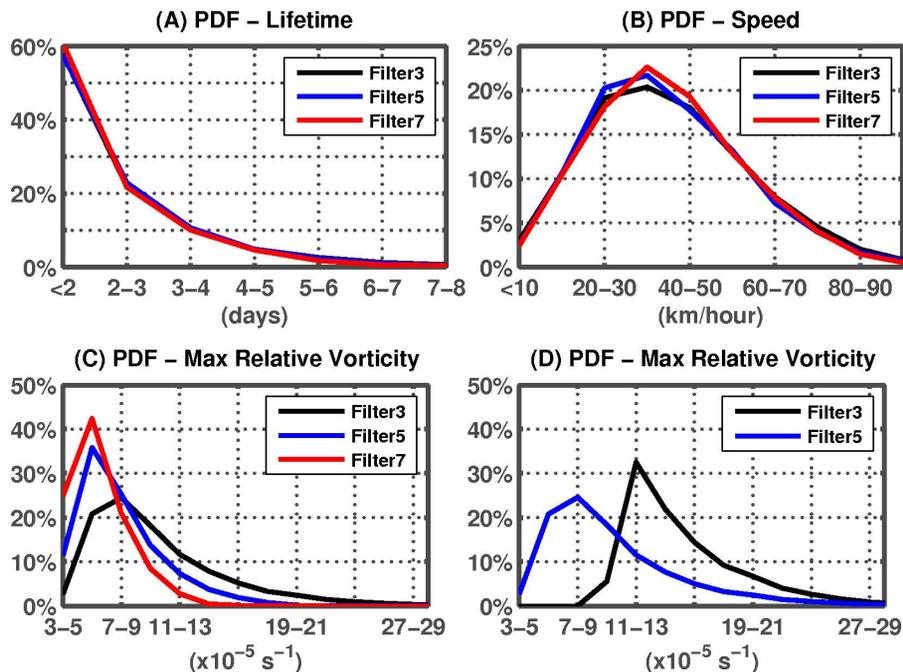
Fig. 7. (A) Probability Distribution Function (PDF) of cyclones life times for the three algorithm integrations. **(B)** As in **(A)** but for cyclones average speed. **(C)** as in **(A)** but for tracks maximum relative vorticity **(D)** as in **(C)** but after excluding tracks that did not reach 10.7 and 5.8 of $\times 10^{-5}\,\mathrm{s}^{-1}$ of relative vorticity in integrations filter3 and filter5, respectively.
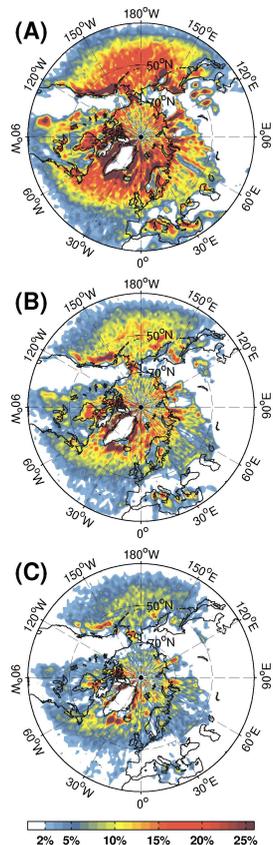
Fig. 8. Cyclone center density expressed as the percentage of cyclone occurrence per time step and per unit area of (1000 km^2) for the **(A)** filter3, **(B)** filter5 and **(C)** filter7 integration.
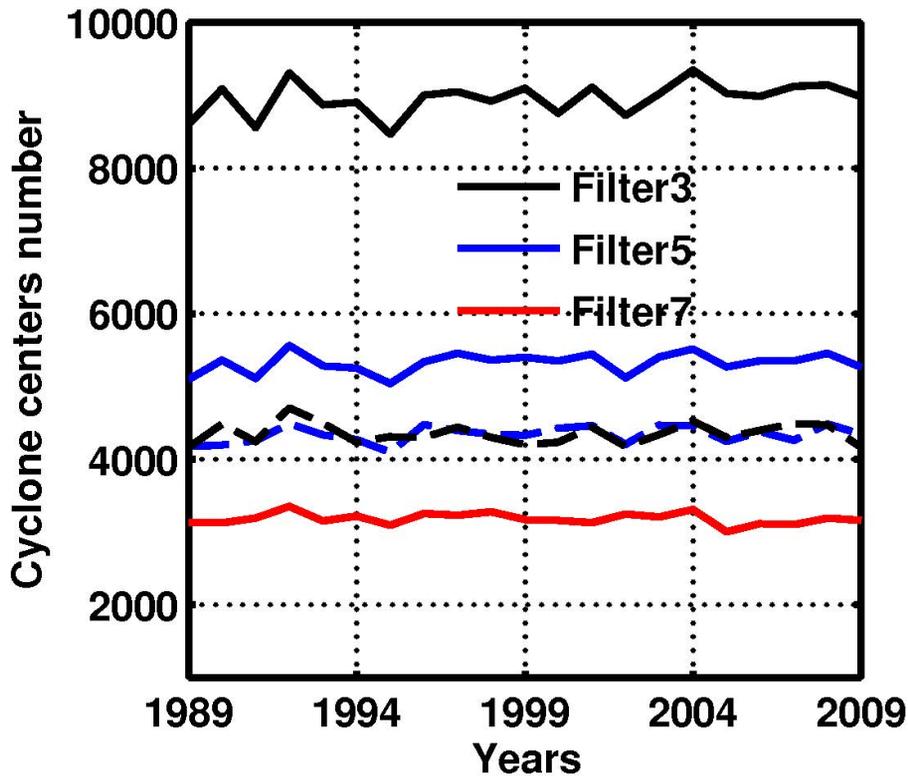
Fig. 9. Number of cyclone centers in function of the year for the three algorithm integrations (black for filter3, gray for filter5 and light grey for filter7). Dashed lines correspond to the integrations filter3 and filter5 after excluding tracks which did not reach a maximum intensity of 10.7 and $5.8 \times 10^{-5} \, \text{s}^{-1}$ of relative vorticity.

Title Page

Abstract | Introduction

Conclusions | References

Tables | Figures

◄ | ►

◄ | ►

Back | Close

Full Screen / Esc

Printer-friendly Version

Interactive Discussion
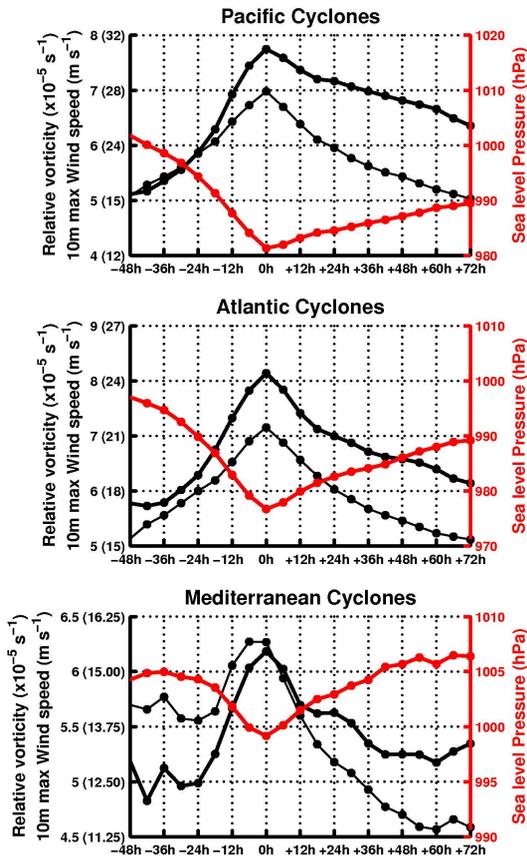
Fig. 10. Average composite time series of cyclones physical characteristics, in three different regions. 0 h corresponds to the time when the cyclone presents its maximum relative vorticity: relative vorticity (thick black line), sea level pressure (red thick line) and maximum 10 m wind speed (thin black line). Wind speed scale values are shown in the left vertical axes in parenthesis. Note that the y-axis has not the same value intervals in the three panels.